Supporting Document

Sustainable and Low-Cost Drinking Water Production via Electrodialysis by Addressing Membrane Fouling Mechanisms to Optimize Cleaning Strategies

Theekshana Malalagama[a,b,c], Binghui Tian[a,b,c]*, R.M.G. Rajapakse[a,b,d], Rehan Gunathilake[a,b,c], Ling Feng[a,b,c],Min Yang[a,b,c]

[a] *National Engineering Research Center of Industrial Wastewater Detoxication and Resource Recovery, Research Center for Eco-Environmental Sciences, Chinese Academy of Sciences, Beijing 100085, China*

[b] *University of Chinese Academy of Sciences, Beijing 100049, China*

[c] *China-Sri Lanka Joint Research and Demonstration Center for Water Technology, Ministry of Water Supply, Meewathura, Peradeniya 20400, Sri Lanka*

[d] *Department of Chemistry, University of Peradeniya, Peradeniya 20400, Sri Lanka*

Correspondence: tianbh@rcees.ac.cn, (Tel: +86- 10-62928390)

SECTION S1: Water quality characteristics of raw and electrodialysis treated groundwater

The raw water was found to contain a significant amount of inorganic matters (Table S1), with multiple parameters exceeding acceptable limits for drinking water. The high electrical conductivity (EC) of 963 μS reflects elevated levels of dissolved solids, indicative of substantial mineral dissolution and prolonged groundwater-rock interactions. Alkalinity and hardness are measured at 600 mg $CaCO_3$/L and 348 mg $CaCO_3$/L, respectively, both far above permissible thresholds, signaling potential scaling and corrosive tendencies in the water. Fluoride, recorded at 4.9 mg/L, poses a particular concern, significantly surpassing the recommended limit and presenting potential health risks with prolonged exposure. Additionally, elevated levels of chloride, sodium, and magnesium point to salinity issues, possibly exacerbated by localized geological and environmental factors. These excessive levels of scale-forming ions, such as calcium and magnesium, increase the likelihood of inorganic fouling in treatment systems, as these ions can precipitate under certain conditions to form scale deposits on membrane surfaces.

Table S1: Properties of groundwater and electrodialysis treated water

Parameter	Unit	Raw water	Treated water
EC	μS	963	204
Alkalinity	mg $CaCO_3$/ L	600	100
Hardness	mg $CaCO_3$/ L	348	53
Cl^-	mg/L	79.8	7.9
NO_3^-	mg/L	5.0	0.7
F^-	mg/L	4.9	0.3
SO_4^{2-}	mg/L	47.7	11.3
Na^+	mg/L	206.1	7.3
K^+	mg/L	1.2	0.4
Ca^{2+}	mg/L	39.8	3.6
Mg^{2+}	mg/L	92.3	8.8
DOC	mg/L	2.562	0.3558
UVA_{254} absorption	cm^{-1}	0.01998	0.00734

The organic matter amount of raw water also significant, as indicated by a DOC concentration of 2.562 ppm and a UV-254 absorbance of 0.0199858. These values suggest a complex mixture of hydrophobic and hydrophilic organic compounds. The relatively low specific UV absorbance (SUVA) of 0.780 L/(mg·m) indicates that the organic matter in the raw water is predominantly non-aromatic and hydrophilic in nature. This aligns with the fluorescence data from the 3D EEM analysis (Figure 6-1), which showed strong fluorescence signals in both protein-like (EX 220–280 nm, EM 300–380 nm) and humic-like (EX 300–350 nm, EM 400–500 nm) regions. The protein-like fluorescence peaks observed in the raw water spectrum point to the presence of recently produced biological organic matter, such as amino acids, peptides, and microbial by-products. These compounds are typically associated with low-molecular-weight, labile organic matter. In contrast, the humic-like fluorescence peaks suggest the presence of high-molecular-weight, aromatic organic compounds derived from natural processes like the decomposition of plant material or soil leachates. The relatively balanced contributions of protein-like and humic-like substances (approximately 30% and 70%, respectively) suggest that the raw water contains both freshly derived organic matter and more refractory humic substances. humic-like substances may lead to organic fouling by forming a dense, adherent layer on membrane surfaces. These organic compounds, in combination with inorganic constituents, could exacerbate membrane fouling, reducing treatment efficiency and increasing maintenance requirements

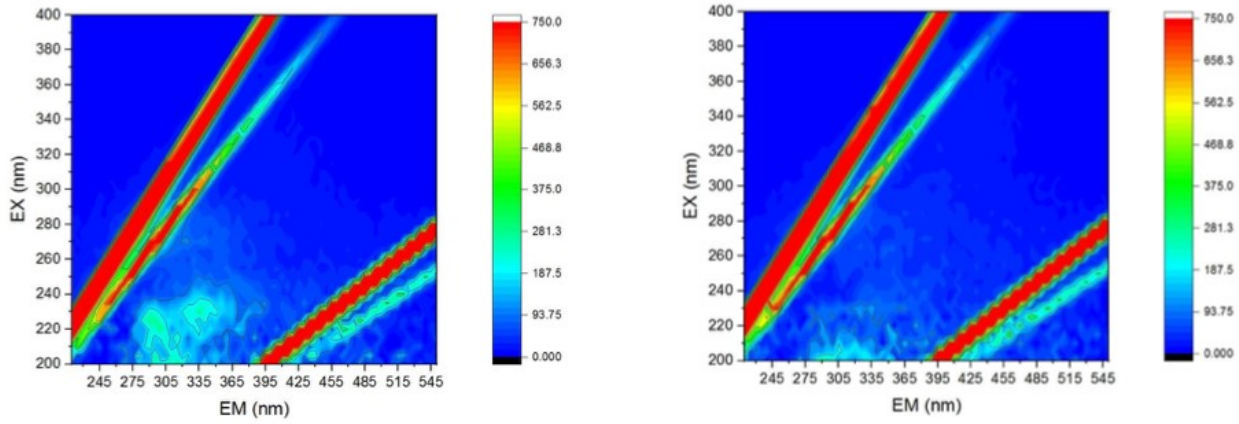

Figure S1: 3D EEMs of (a) raw and (b) treated water by electrodialysis

The ED treatment significantly enhanced water quality by effectively reducing the concentrations of key contaminants, demonstrating its efficiency as an ion-selective removal technology. Fluoride levels were reduced by 93.88%, highlighting the system's capability to target

and remove specific ions. Hardness also showed substantial improvement, with an 84.77% reduction, effectively mitigating scaling risks. Additionally, EC, alkalinity, and sulfate levels were reduced by 78.8%, 83.33%, and 76.32%, respectively, further indicating the ED system's ability to address a broad spectrum of water quality challenges. Reductions in scale-forming ions such as magnesium (90.46%) and calcium (90.95%) were equally notable, ensuring the treated water's suitability for consumption and preventing issues related to scaling and hardness. In addition to inorganic ion removal, the ED system exhibited remarkable efficiency in addressing organic matter contamination. The DOC concentration decreased by 86.1%, from 2.562 ppm to 0.3558 ppm, while the UV-254 absorbance dropped by 63.3%, from 0.0199858 to 0.0073365. The more pronounced reduction in DOC compared to UV-254 suggests that the ED process preferentially removed non-aromatic, hydrophilic organic compounds, which constitute a major fraction of the raw water organics. This finding aligns with the low SUVA value of the raw water, indicating that the treated water was effectively purified not only of ions but also of organic contaminants, rendering it safe for consumption and significantly improving its overall quality.

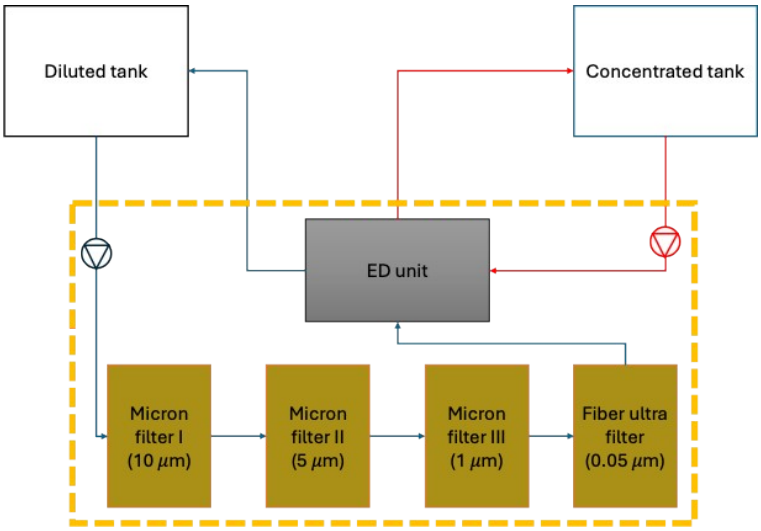

Figure S2: Schematic diagram of the laboratory setup used for the experiment.

Figure S3: Visual inspection of virgin (a) and fouled ((b) diluted side and (c) concentrated side) elements CEM

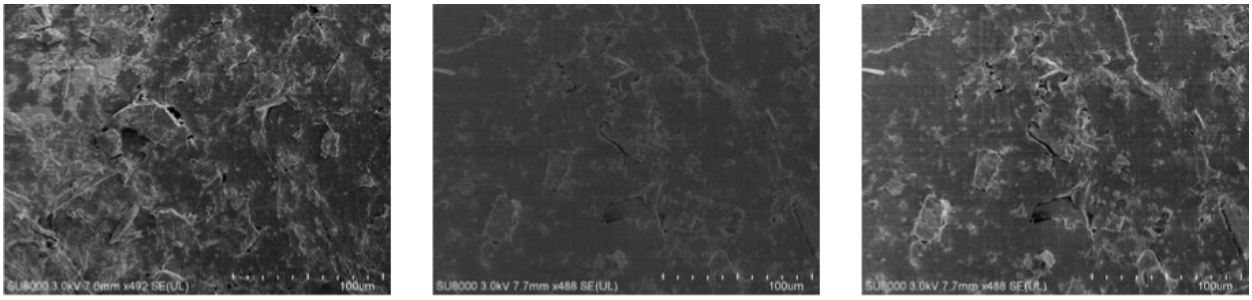

Figure S4: Magnified SEM image of fouled CEM surface

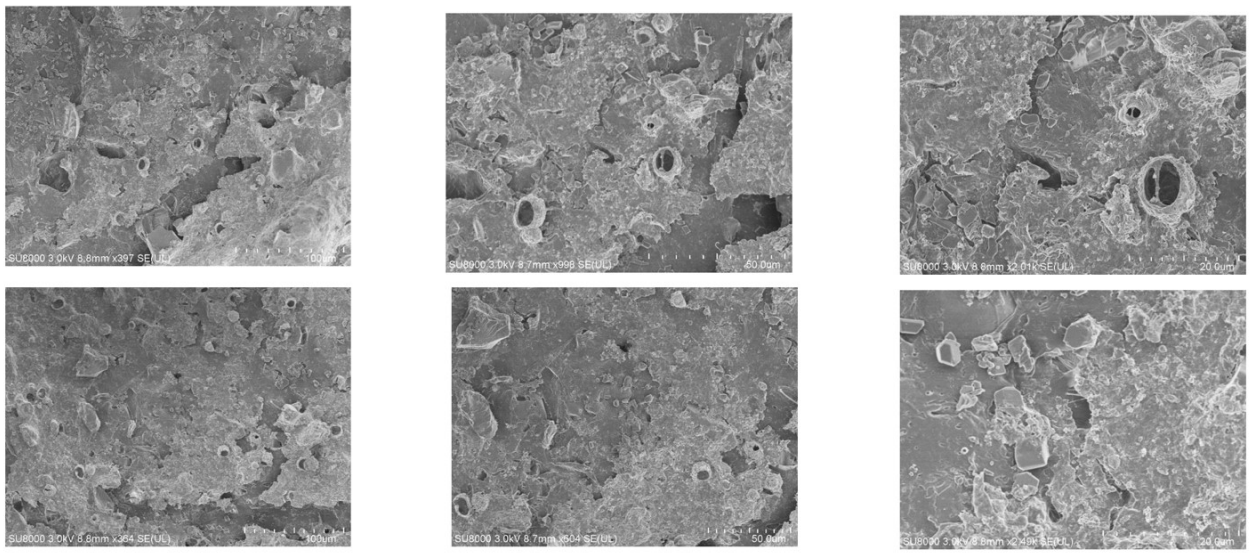

Figure S5: Magnified SEM image of fouled AEM surface

SECTION S2: Fouling morphology and composition of IEMs

S2.1: SEM/ EDS analysis of the fouled membrane elements

As shown in Figure S6 (Table S2) the most available elements in the fouled membranes are C > O > Ca > Si = Mg = S in AEM.

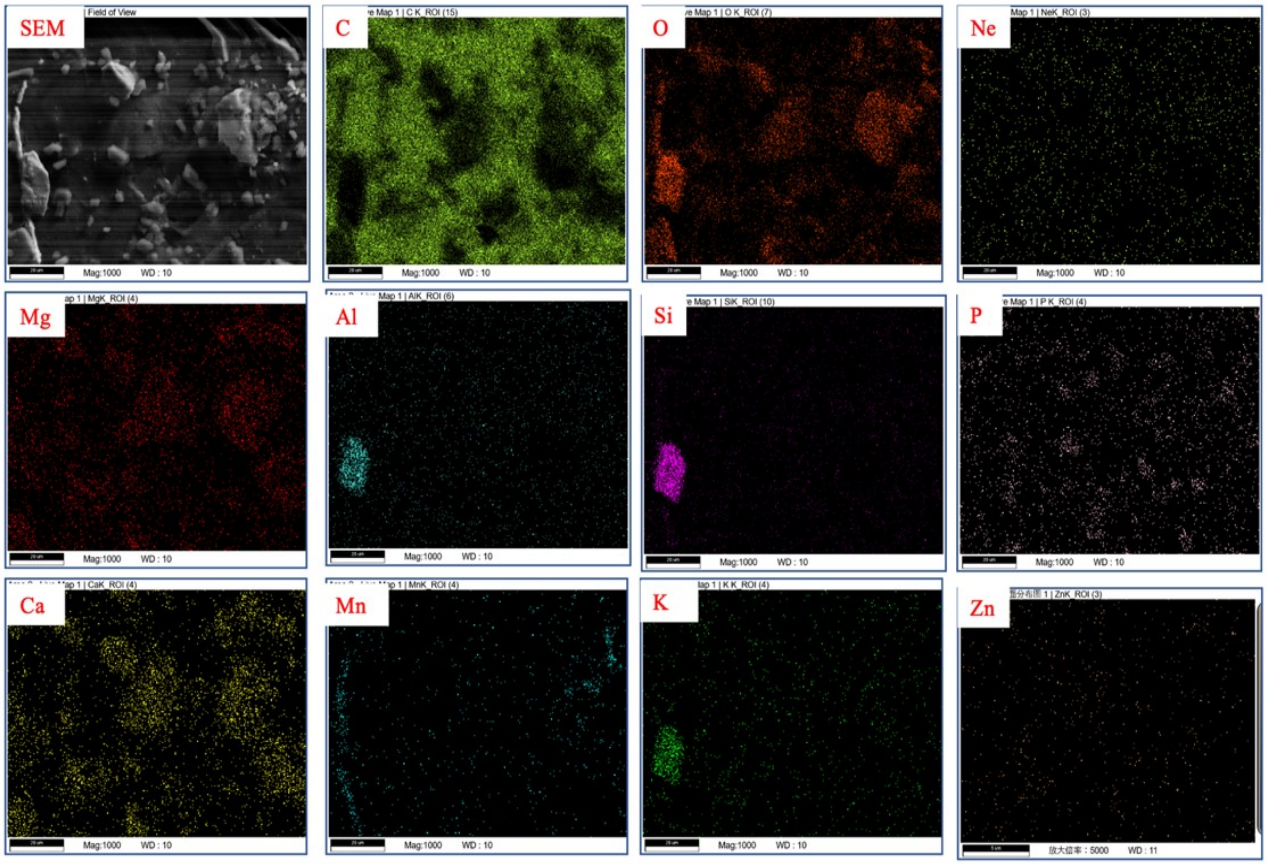

Figure S6: The element distribution in fouled AEM of EDS analysis

Table S2:EDS elemental analysis of fouled AEM

eZAF Quant Result – Analysis Uncertainty: 10.07 %								
Element	Weight %	MDL	Atomic %	Error %	Net Int.	R	A	F
C K	87.1	0.07	91.6	8.4	3770.6	0.9402	0.2970	1.0000
O K	8.7	0.12	6.8	12.0	323.3	0.9482	0.1028	1.0000
Ne K	0.1	0.02	0.1	21.9	16.5	0.9544	0.3392	1.0000
Na K	0.2	0.03	0.1	10.5	40.6	0.9572	0.5042	1.0019
Mg K	0.4	0.02	0.1	7.1	80.9	0.9600	0.6541	1.0030
Al K	0.1	0.02	0.1	9.1	39.2	0.9625	0.7651	1.0048
Si K	0.4	0.02	0.1	6.0	69.7	0.9649	0.8425	1.0070
P K	0.1	0.02	0.1	9.4	37.2	0.9672	0.8942	1.0105
S K	0.4	0.02	0.6	3.2	388.2	0.9693	0.9263	1.0111
K K	0.1	0.03	0.0	16.8	17.0	0.9752	0.9706	1.0299
Ca K	1.2	0.04	0.2	5.3	95.7	0.9770	0.9788	1.0325
Mn K	0.2	0.07	0.0	29.0	10.8	0.9854	0.9952	1.1184
Au M	0.2	0.07	0.0	14.2	39.8	0.9692	0.9209	1.0156

Some of these elements were deposited as crystals at some locations. Needle-like crystals and block crystals are observed for salts of Ca and Mg deposited as these elements are present contributing to the hardness in groundwater.

The presence of significant amount of Ca and Mg with C and O elements are indicated that, membrane surface is covered by scaling assured to be precipitated as $CaCO_3$ and $MgCO_3$. However, these precipitated materials along the membrane are distributed in different patterns though the constitute elements are same. The precipitated Ca and Mg were dense and scattered in vast area. Another type of needle type crystals include~~d~~ the abundance of several inorganic elements such as Si, Al, consisting of O as their oxides. The presence of Si and Al are thought to originate from groundwater. Previous research has been identified that Sri Lanka's NCP groundwater contains considerable amount of Si though Al concentration is significantly less. Gorzalski, A.S., 2014 has identified that silica in groundwater is also dominant in membrane

fouling [1] which supports our results. It is also suggesting that aluminum silicate compounds also acting as foulants. Ohno K., 2010 revealed that, even though the concentration of aluminum is not too high, excessive amount of silicate and less amount of aluminum caused on membrane foulant as alumino-silicates or aluminum hydroxide which is consistent with our observations in this research as there are some Al spots on the membrane surface [2]. Silt, clay quartz and sand particles which contain high amount of silica association with trivalent and divalent cations (Fe_2SiO_4, Al_2SiO_5 and Mg_2SiO_4) would be some forms of depositions on membranes. The solubilities of these compounds are much lower than the pure silca and formation of these salts is usually promoted by the incorrect use of anti-scalants [3], [4]. Mn, Fe, S, P, Zn, K also can be seen as depositions on membrane surface which supports the presence of other inorganic foulant/ scale material on the membrane surface other than previously discussed major foulants/ scale materials. Most of these salts tend to increase the coverage area reducing porosity and thereby reducing flux through membranes [5].

SEM images shown in Figure 2 clearly show a fracture that is probably caused by the drying procedure used.

S2.2 XRD analysis of the foulant

The XRD analysis was employed to conduct a comprehensive characterization of the fouling species on the IEMs. As depicted in Figure S7, a distinct pattern emerged, revealing the presence of multiple peaks clustered around 25° in the AEM. Notably, five specific peaks at 17.98 (140), 20.2 (130), 21.6 (111), 22.82, and 25.76 were identified within this region, characteristics well-documented in the literature as indicative of polypropylene material [6]. Moreover, the analysis disclosed a series of peaks scattered between 25° and 50° angles, each representing distinct crystallographic planes within the sample [7]. This array of peaks provided compelling evidence of $CaCO_3$ formation, with pronounced calcite and vaterite peaks spanning the entire 25° to 50° range including ($CaMg(CO_3)_2$) peaks [8], [9], while aragonite peaks appeared at 26.8°, 31.09°, and 45.86°[10]. These findings were consistent with observations from SEM images (Figure 6-5). Notably, the XRD data unveiled the presence of quartz (SiO_2) peaks in Figure S7, affirming the existence of prominent silicate crystalline foulants adhering to the membrane surface

[11]. This detailed XRD analysis thus serves as a key component in unraveling the complex nature of the fouling species present on the membranes.

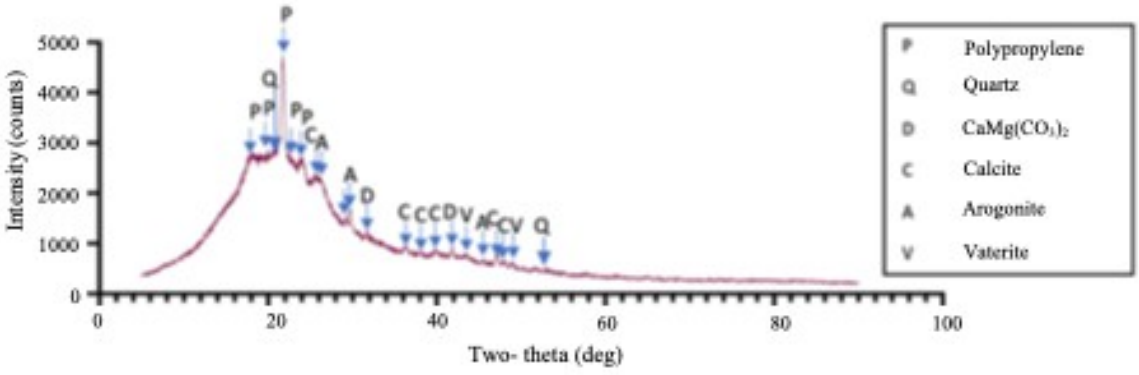

Figure S7: X-ray diffraction (XRD) analysis results of fouling in AEM

The width of peaks observed in the XRD analysis is a crucial indicator of crystallite size, with broader peaks suggesting smaller crystallite dimensions, as documented in prior research [6]. Our analysis revealed that the size of the newly formed crystals encompassed a spectrum of dimensions, as evidenced by the range of peak widths displayed in Figure S7. Specifically, the AEM demonstrated the creation of larger crystallites. This distinction is readily apparent when examining the SEM images showcased in Figure 3 (in main document). It is important to note that while XRD analysis provides valuable insights into crystallinity, it has limitations in distinguishing among various components, such as bulky, amorphous, fouling, or colloidal materials, within the sample. This underscores the need for complementary analytical techniques to fully elucidate the diverse nature of components present in the fouling layer.

S2.3 FTIR analysis of fouled membrane

FTIR analysis were conducted to determine the inorganic fouling layers qualitatively on the membrane surfaces. The spectra of fouled AEM were shown at Figure S8. FTIR spectrum of various crystal forms of calcium carbonate ($CaCO_3$) indeed exhibits distinct bands associated with the unique vibrational modes of different polymorphs of $CaCO_3$, including calcite, aragonite, and

vaterite. These polymorphs have different crystal structures, and their vibrational modes result in characteristic bands in the FTIR spectrum. The presence of $CaCO_3$ fouling on a membrane can be identified by observing these distinctive vibrations. One of the three primary polymorphs of $CaCO_3$, aragonite, exhibits carbonate out-of-plane bending in one of these bands, with a vibration at 855.26 cm^{-1}[12]. The v2 mode of carbonate out-of-plane bending vibrations, which are caused by both calcite and vaterite polymorphs, are also present at 879.1 cm^{-1}[13]. This common feature arises from the distinctive crystal structures of these polymorphs. The carbonate groups in $CaCO_3$ also show strong vibrational oscillations, as indicated by a prominent peak at 1392.6 cm^{-1}. All these several characteristic vibrations are consisting with $CaCO_3$ fouling on the membrane. The band on 1082 cm^{-1} revealed that calcite has incorporated with Mg [14].

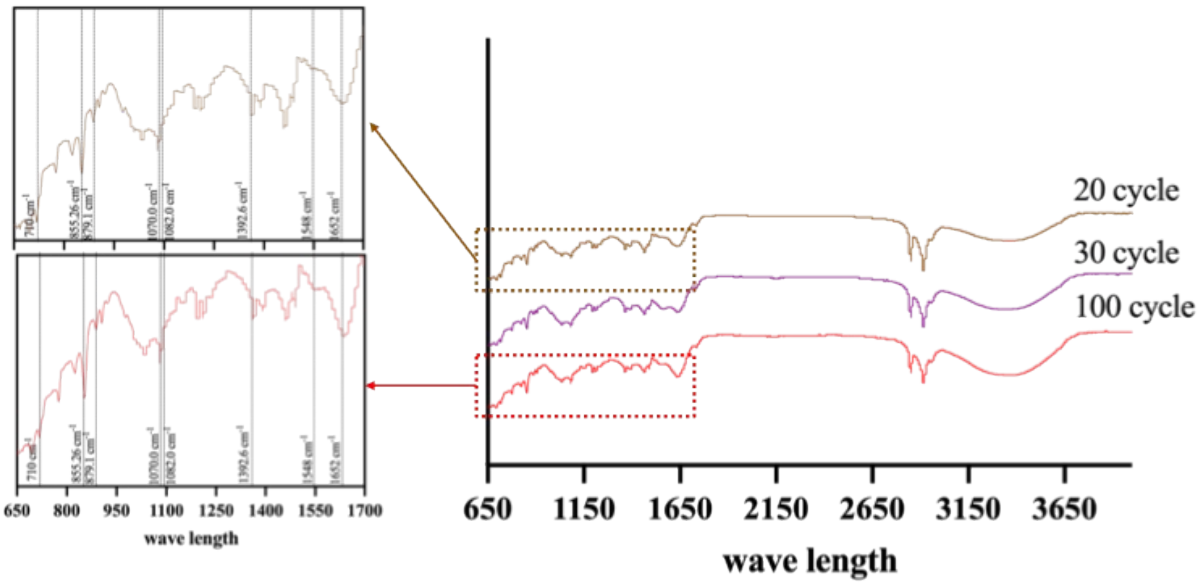

Figure S8: Fourier Transformation Infrared Spectroscopy (FTIR) spectra of AEM.

The presence of a silicate foulant on the membrane has been unequivocally verified through detailed examination of FTIR spectra. In our analysis, we observed a spectrum analogous to that of pure SiO_2, notably featuring a distinct absorption band at 710 cm^{-1}. This particular band, found at 710 cm^{-1}, is attributed to the symmetric vibration of the Si–O bond, mirroring the experimental results and aligning perfectly with the anticipated spectral signature of SiO_2, thus reinforcing our identification. Further scrutinizing the FTIR spectrum, we identified another crucial feature. The Si-O-Si stretching vibrations, a prominent hallmark in the spectrum of SiO_2 in its various forms,

were discernible in the range of 1050-1100 cm^{-1}. Notably, the broad peak at approximately 1050 cm^{-1}, known for its association with the absorption of Si-OH or SO_4^{2-}, displayed a broadening effect when compared between the fouled membrane and the pristine precipitate [15]. This broadening trend signifies the presence of more intricate compositions within the fouling material, hinting at a complex interplay of chemical constituents and reinforcing the multifaceted nature of silicate fouling on the membrane surface.

In addition to the aforementioned findings, the FTIR spectra revealed valuable insights into the presence of biofouling on the membrane. Notably, we detected relatively modest yet distinct peaks that shed light on the existence of key biomolecular constituents. In each spectrum, prominent peaks indicative of glycan chains (notably at 1070 and 2840 cm^{-1}) and amides, especially those associated with biogenic foulant proteins (Amide I and II, observed at 1652 and 1548 cm^{-1}), underscored the pivotal roles of polysaccharides and proteins as the primary organic membrane foulants.

A particularly noteworthy absorption peak near 1082.2 cm^{-1} emerged as a significant clue. This peak is linked to C–C and C–O stretching vibrations, offering strong support for the concept of cross-linking between polysaccharides and calcium [13]. This observation reinforces the intricate nature of biofouling and highlights its active development in the context of membrane fouling during the ED desalination process. The interplay of glycan chains, amides, and the bonding between polysaccharides and calcium further underscores the complex composition and dynamics of biofouling in membrane systems.

S2.4 XPS analysis of fouled membrane

IEM foulants were subjected to XPS analysis in order to determine their chemical composition, chemical states, surface concentration, and electronic structure. In accordance with the findings of the EDS, the top four elements were oxygen, carbon, calcium, and magnesium. In the C spectra, three peaks can be observed; located at 289.50 eV, 285.64 eV, and 284.74 eV respectively. These are indicating the combination of inorganic and organic foulant bonded as CO_3^{2-}, C—O and C—C [12]. The O spectra displayed two different peaks, one at 531.75 eV and the other at 533.23 eV. These peaks, which corresponded to carbonates and O—C bonds [13]. The

Ca spectra showed two peaks at 439.6eV and 347.07eV. These peaks were assigned to the 2p3/2 and 2p1/2 orbitals, and calcium carbonate was determined to be the substance responsible for them [16]. The Mg spectrum had one single peak placed around 1304 eV that was attributed to the Mg(II) ions. This peak was determined to be $MgCO_3$. The presence of a second, much smaller peak of magnesium at 302.7 eV, which can be attributed to the Mg—O bond, further confirms the deposition of magnesium throughout the scaling process. The overall XPS study provided evidence that the predominant scaling component on membranes was composed of $CaCO_3$ and $MgCO_3$. In addition to the peaks discussed above, a peak that is approximately at 101.2 eV and attributed to a Si—O bond can be observed. This peak suggests that SiO_2 is present on the membrane [17]

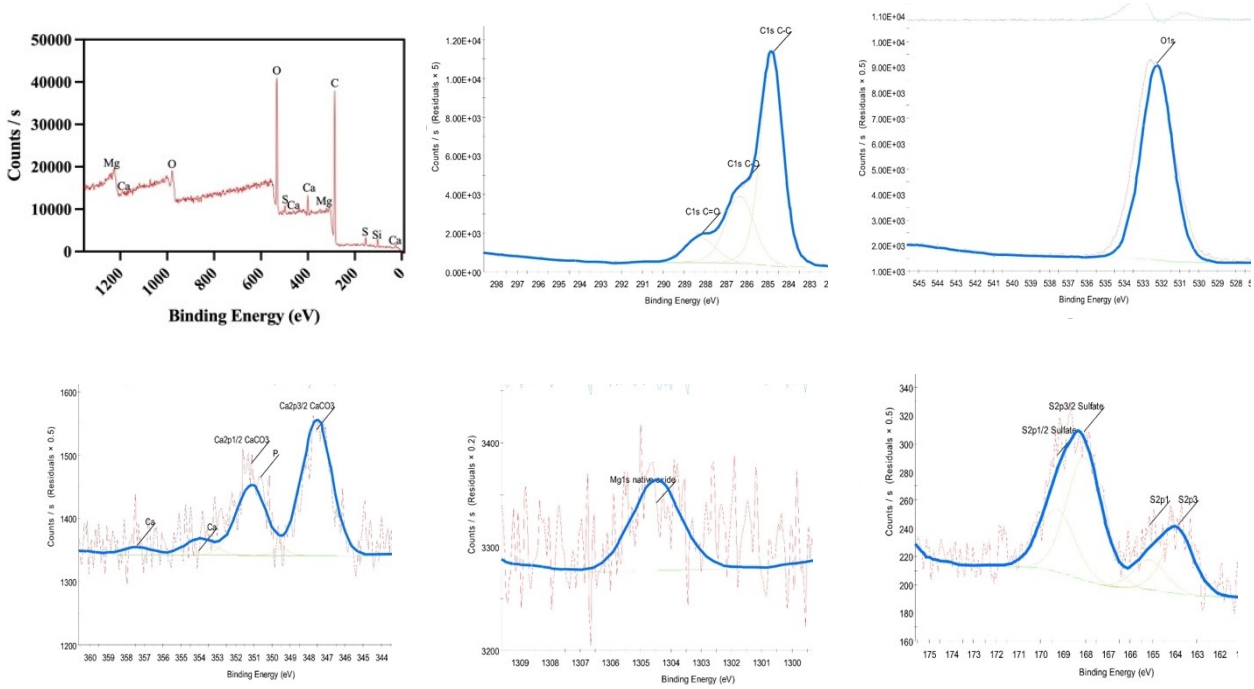

Figure S9: The full XPS spectrum and C[1]s, O[1]s, Ca[2]P, Ca[2]s, Mg[1]s, F[1]s and S[2]p spectra of the fouled AEM

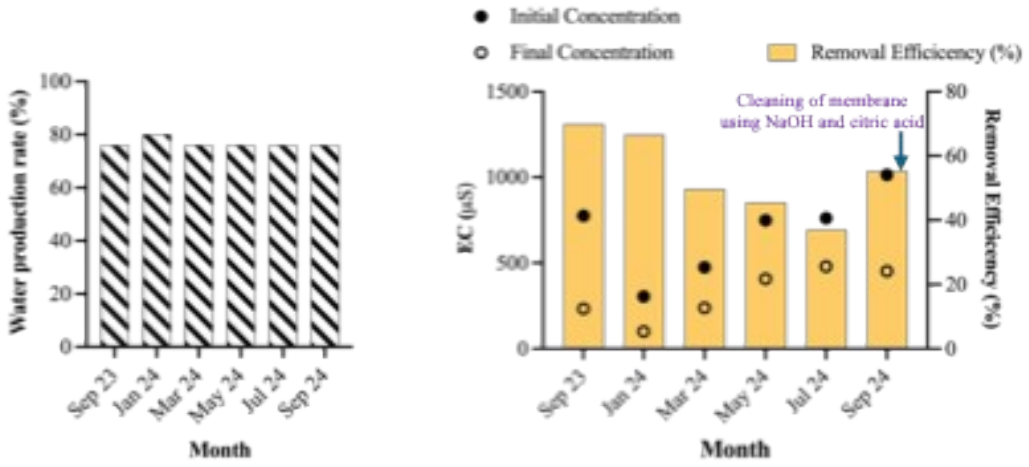

Figure S10: (a). Water production rate (%) and (b). variation of electrical conductivity of ED run in Padaviya, Anuradhapura

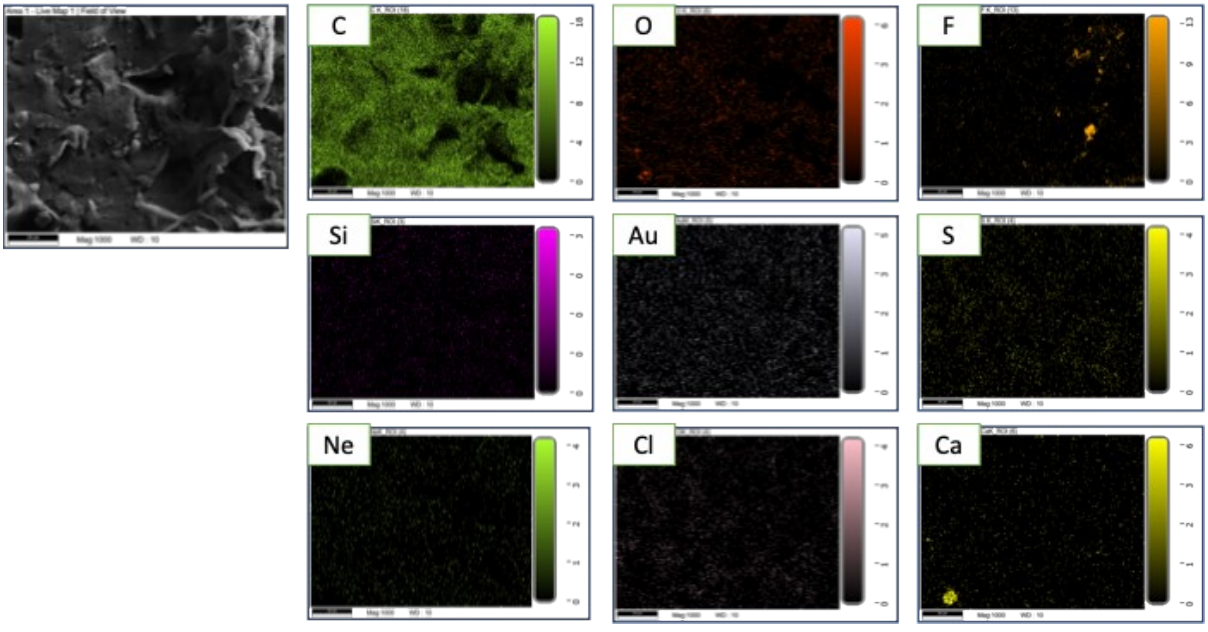

Figure S11: The EDS-mapping of cleaning by HCl

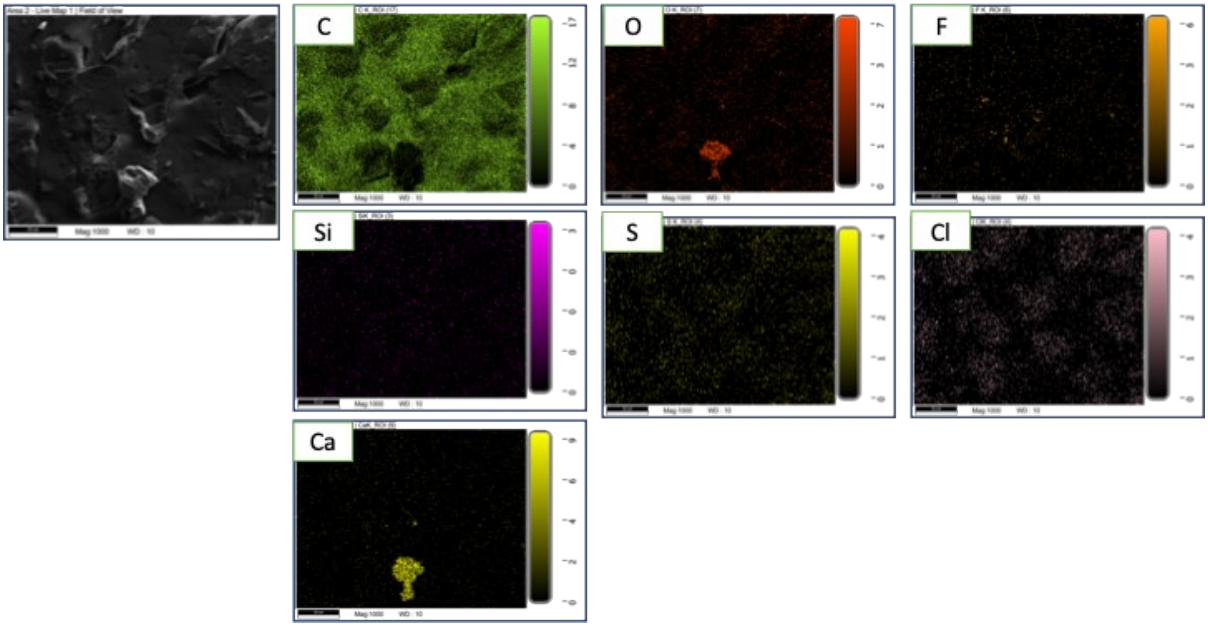

Figure S12:The EDS-mapping of cleaning by NaOH

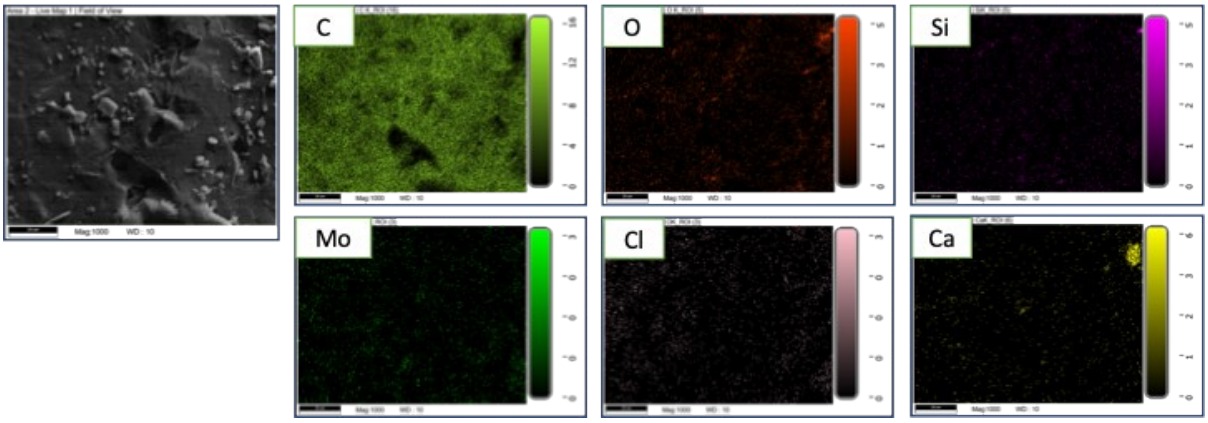

Figure S13: The EDS-mapping of cleaning by DW

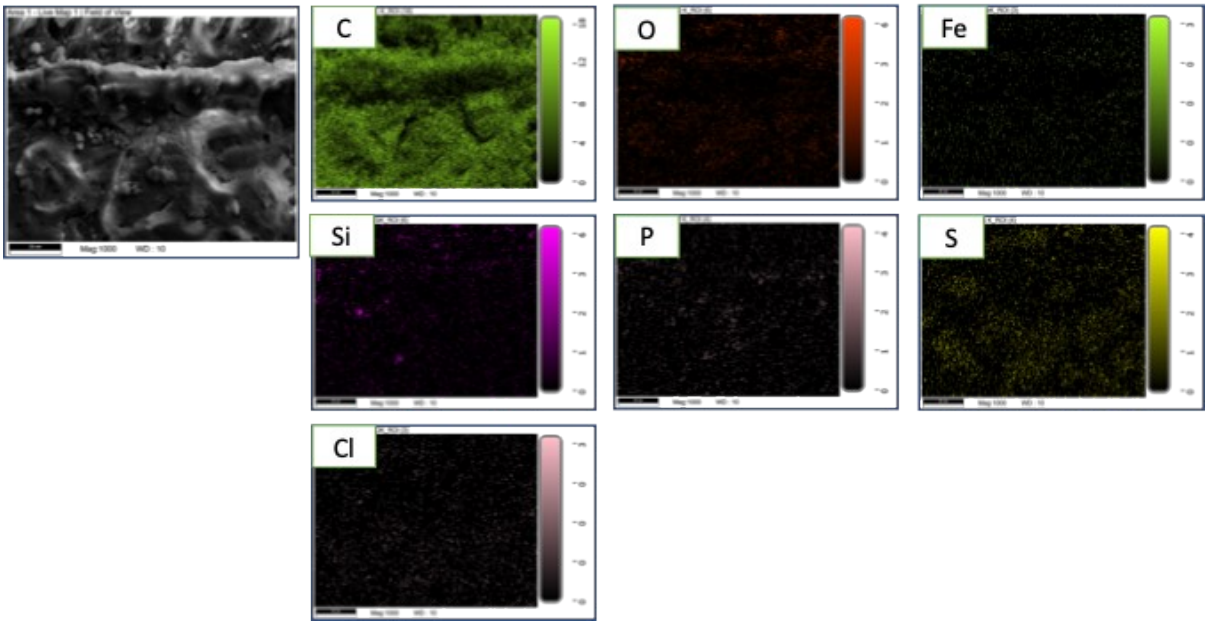

Figure S14: The EDS-mapping of cleaning by HAc

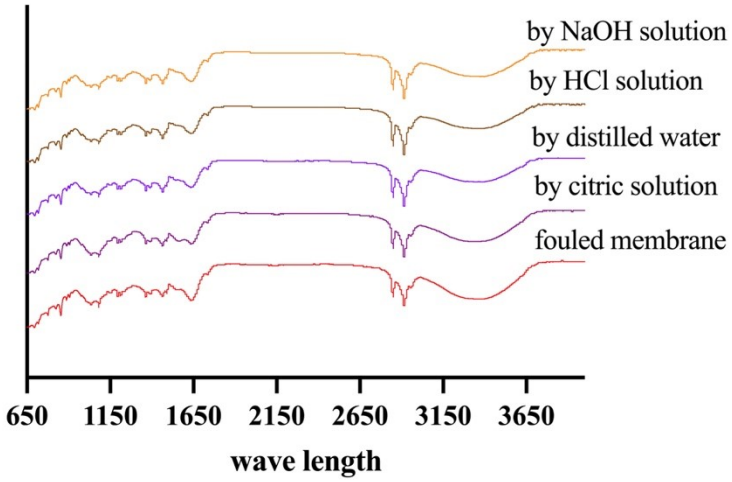

Figure S15: Fourier Transformation Infrared Spectroscopy (FTIR) spectra of cleaned AEMs. By different solutions

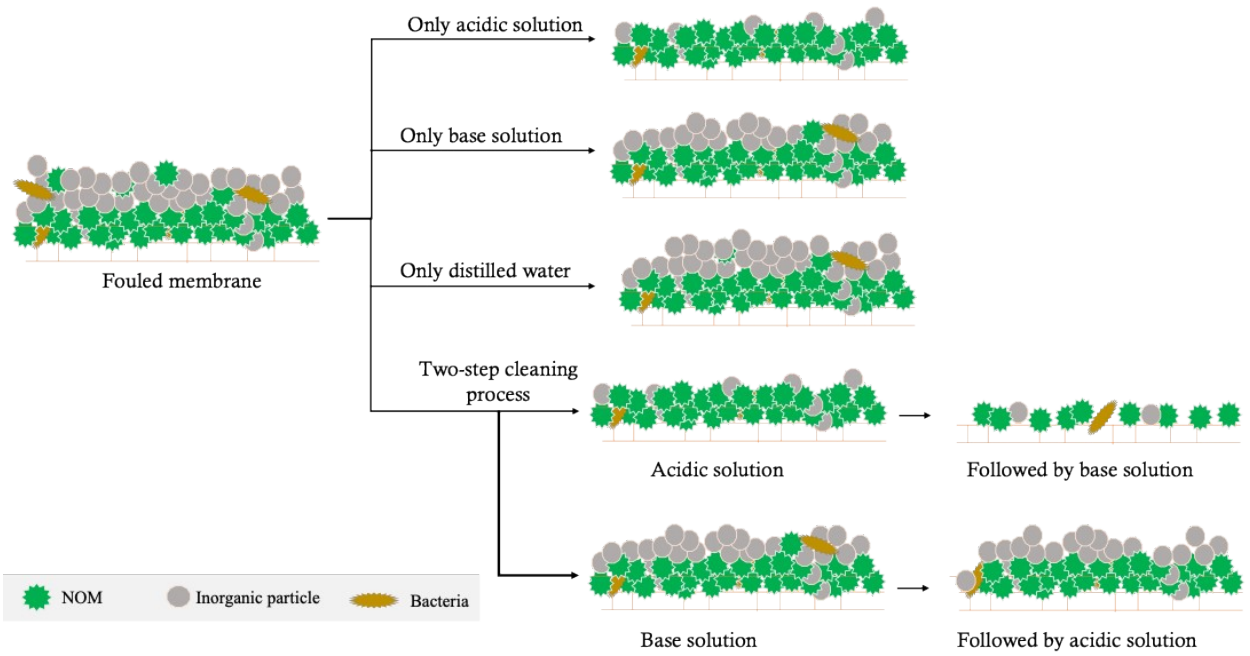

Figure S16: Effectiveness of different cleaning stratergies

References

[1] A. S. Gorzalski and O. Coronell, "Fouling of nanofiltration membranes in full- and bench-scale systems treating groundwater containing silica," *J Memb Sci*, vol. 468, pp. 349–359, Oct. 2014, doi: 10.1016/j.memsci.2014.06.013.

[2] K. Ohno *et al.*, "NF membrane fouling by aluminum and iron coagulant residuals after coagulation–MF pretreatment," *Desalination*, vol. 254, no. 1–3, pp. 17–22, May 2010, doi: 10.1016/j.desal.2009.12.020.

[3] Y. Tapiero, F. Mery, and A. García, "Understanding of surface fouling of brackish water reverse osmosis spiral wound membrane using an integrated analysis of seawater quality and membrane autopsy," *Chem Eng Sci*, vol. 280, p. 119028, Oct. 2023, doi: 10.1016/j.ces.2023.119028.

[4] L. Fortunato, A. H. Alshahri, A. S. F. Farinha, I. Zakzouk, S. Jeong, and T. Leiknes, "Fouling investigation of a full-scale seawater reverse osmosis desalination (SWRO) plant on the Red Sea: Membrane autopsy and pretreatment efficiency," *Desalination*, vol. 496, p. 114536, Dec. 2020, doi: 10.1016/j.desal.2020.114536.

[5] X. Tang *et al.*, "Respective role of iron and manganese in direct ultrafiltration: from membrane fouling to flux improvements," *Sep Purif Technol*, vol. 259, p. 118174, Mar. 2021, doi: 10.1016/j.seppur.2020.118174.

[6] D. Akbar, “Surface modification of polypropylene (PP) using single and dual high radio frequency capacitive coupled argon plasma discharge,” *Appl Surf Sci*, vol. 362, pp. 63–69, Jan. 2016, doi: 10.1016/j.apsusc.2015.11.191.

[7] D. Akbar, “Surface modification of polypropylene (PP) using single and dual high radio frequency capacitive coupled argon plasma discharge,” *Appl Surf Sci*, vol. 362, pp. 63–69, Jan. 2016, doi: 10.1016/j.apsusc.2015.11.191.

[8] M. Adel, T. Nada, S. Amin, T. Anwar, and A. A. Mohamed, “Characterization of fouling for a full-scale seawater reverse osmosis plant on the Mediterranean sea: membrane autopsy and chemical cleaning efficiency,” *Groundw Sustain Dev*, vol. 16, p. 100704, Feb. 2022, doi: 10.1016/j.gsd.2021.100704.

[9] R. Febrida, S. Setianto, E. Herda, A. Cahyanto, and I. M. Joni, “Structure and phase analysis of calcium carbonate powder prepared by a simple solution method,” *Heliyon*, vol. 7, no. 11, p. e08344, Nov. 2021, doi: 10.1016/j.heliyon.2021.e08344.

[10] Md. Sahadat Hossain and S. Ahmed, “Crystallographic characterization of naturally occurring aragonite and calcite phase: Rietveld refinement,” *Journal of Saudi Chemical Society*, vol. 27, no. 3, p. 101649, May 2023, doi: 10.1016/j.jscs.2023.101649.

[11] Y. Zhao *et al.*, “Self-assembled embedding of ion exchange materials into nanofiber-based hydrogel framework for fluoride capture,” *Chemical Engineering Journal*, vol. 431, p. 134201, Aug. 2022, doi: 10.1016/j.cej.2021.134201.

[12] S. Wang, Y. You, X. Wang, W. Huang, L. Zheng, and F. Li, “Fouling mechanism and effective cleaning strategies for vacuum membrane distillation in brackish water treatment,” *Desalination*, vol. 565, p. 116884, Nov. 2023, doi: 10.1016/j.desal.2023.116884.

[13] M. Khanjani, D. J. Westenberg, A. Kumar, and H. Ma, “Tuning Polymorphs and Morphology of Microbially Induced Calcium Carbonate: Controlling Factors and Underlying Mechanisms,” *ACS Omega*, vol. 6, no. 18, pp. 11988–12003, May 2021, doi: 10.1021/acsomega.1c00559.

[14] B. Purgstaller, V. Mavromatis, A. Immenhauser, and M. Dietzel, “Transformation of Mg-bearing amorphous calcium carbonate to Mg-calcite – In situ monitoring,” *Geochim Cosmochim Acta*, vol. 174, pp. 180–195, Feb. 2016, doi: 10.1016/j.gca.2015.10.030.

[15] Y. Liu, H. Zhang, C. Jiang, X. Jiang, T. Sakamaki, and X. Li, “Effect of bio-electrochemical systems on the removal of organic and inorganic membrane fouling from anaerobic membrane bioreactors,” *Sep Purif Technol*, vol. 312, p. 123395, May 2023, doi: 10.1016/j.seppur.2023.123395.

[16] Chen Yipeng *et al.*, “The properties of fibreboard based on nanolignocelluloses/CaCO3/PMMA composite synthesized through mechano-chemical method. ,” Hangzhou, Zhejiang Province, China, Mar. 2018.

[17] Michel C, Emmanuel M, Michel L, Nathalie H, Xavier A, and Martine M, *Nano structured Silicon-based Powders and Composites*, 1st ed. London: Taylor and Francis, 2003.